HHS Public Access

Author manuscript

J Theor Biol. Author manuscript; available in PMC 2019 November 18.

Published in final edited form as:

J Theor Biol. 2012 June 21; 303: 141–151. doi:10.1016/j.jtbi.2012.03.024.

Modeling the inhibition of breast cancer growth by GM-CSF

Barbara Szomolay[b,*], **Tim D. Eubank**[a], **Ryan D. Roberts**[a], **Clay B. Marsh**[a], **Avner Friedman**[b,c]

[a]Division of Pulmonary, Allergy, Critical Care & Sleep Medicine, College of Medicine, The Ohio State University, United States

[b]Mathematical Biosciences Institute, The Ohio State University, United States

[c]Department of Mathematics, The Ohio State University, United States

Abstract

M-CSF is overexpressed in breast cancer and is known to stimulate macrophages to produce VEGF resulting in angiogenesis. It has recently been shown that the growth factor GM-CSF injected into murine breast tumors slowed tumor growth by secreting soluble VEGF receptor-1 (sVEGFR-1) that binds and inactivates VEGF. This study presents a mathematical model that includes all the components above, as well as MCP-1, tumor cells, and oxygen. The model simulations are representative of the *in vivo* data through predictions of tumor growth using different protocol strategies for GM-CSF for the purpose of predicting higher degrees of treatment success. For example, our model predicts that once a week dosing of GM-CSF would be less effective than daily, twice a week, or three times a week treatment because of the presence of essential factors required for the anti-tumor effect of GM-CSF.

Keywords

Mathematical modeling; Angiogenesis

1. Introduction

Macrophages play an essential role in normal breast development, especially during pregnancy and lactation (Pollard, 1997), but also during the development and progression of breast tumors. It has been reported that the macrophage survival and differentiation factor, macrophage colony-stimulating factor (M-CSF), are overexpressed in over 70% of human breast cancers (Sapi, 2004). Correspondingly, mice deficient in M-CSF is protected against breast tumor metastasis while overexpression of M-CSF in these same mice recovered tumor metastasis to the lung (Lin et al., 2001).

It was shown by Eubank et al. (2003) that M-CSF induces monocytes and macrophages to produce biologically-active vascular endothelial growth factor (VEGF), thereby mobilizing endothelial cells and inducing angiogenesis. In breast tumors, these tumor-associated macrophages (TAMs) constitute up to 35% of infiltrating inflammatory cells (Tang et al.,

*Corresponding author. Current address: Mathematics Institute, University of Warwick, United Kingdom. Tel.: +44 7727427786. b.szomolay@warwick.ac.uk (B. Szomolay).

1992) and reside mostly in hypoxic regions of the tumor core—clearing dead cell debris. TAMs are recruited into the tumors by monocyte chemoattractant protein-1 (MCP-1) which is released from both stromal cells and tumor cells (Fujimoto et al., 2009). Interestingly, depending on their polarity, either M1- or M2-type macrophages can play two different roles in the regulation of tumor growth. On the one hand, M1 macrophages produce high levels of interleukins IL-12, IL-23, IL-1, IL-6, TNFa, the chemokine CXCL10, inducible nitric oxide synthase (iNOS), human leukocyte antigen (HLA)-DR, reactive oxygen and nitrogen that help fight tumor growth (Mantovani et al., 2007, 2005; Baj-Krzyworzeka et al., 2007; Mantovani et al., 2002). On the other hand, M2 macrophages express high levels of IL-10, IL-ra, CCL22, scavenger, mannose and galactose receptors, arginase I, CD163 antigen, matrix metalloproteinases (MMPs), and VEGF which serve to help tumor progression (Mantovani et al., 2007; Gordon, 2003; Hagemann et al., 2004).

In a follow-up to their report showing that the growth factor granulocyte/macrophage colony-stimulating factor (GM-CSF) induces monocytes to secrete soluble VEGF receptor-1 (sVEGFR-1) which binds to and inactivates VEGF (Eubank et al., 2004), Eubank et al. (2008) investigated the hypothesis that macrophage phenotype and behavior in breast tumors can be manipulated *in vivo* by GM-CSF. It was previously known that GM-CSF can enhance the ability of macrophages to present antigen and initiate an immune response (Armstrong et al., 1996). In the study (Eubank et al., 2008), MET-1 mammary tumor cells were orthotopically-injected into normal female FVB/N mice. After tumors became palpable (approximately 28 days after seeding), 100 ng GM-CSF was injected directly into the tumors three times a week. Treatment with GM-CSF reduced tumor growth and metastasis; moreover, GM-CSF lowered oxygen tension and reduced blood vessel density within the tumor by suppressing angiogenic activity. Further, Eubank et al. (2008) showed that tumors treated with GM-CSF had more TAMs of an M1 polarity while vehicle-treated tumors had more M2-type and support the role of GM-CSF contributing to an M1 phenotype (Mantovani et al., 2007). The experimental data also demonstrated that GM-CSF reversed some of the pro-tumor “education” of immune cells driven by tumor cell:macrophage interaction and induced a more anti-tumor phenotype from the TAMs.

There have been a number of mathematical studies modeling the macrophage infiltration into avascular tumors (Owen and Sherratt, 1997; Kelly et al., 2002; Owen et al., 2004), i.e., a tumor small enough to be able to satisfy its nutritional needs by diffusion from nearby blood vessels. These studies focused either on the possibility of spatial pattern formation within the growing tumor (Owen and Sherratt, 1997), or on the dependence of the macrophage infiltration pattern on the motility mechanisms (random motion, chemotaxis) (Armstrong et al., 1996). Macrophage chemotactic sensitivity has been shown to be a key determinant of macrophage infiltration and tumor size (Kelly et al., 2002; Owen et al., 2004). Increased infiltration should be beneficial in the context of macrophage-based therapies; however, such infiltration in fact leads to increased tumor size (Kelly et al., 2002).

In the present study, we develop a mathematical model to predict the effect of GM-CSF treatment on tumor growth in a mouse model of breast cancer. The model takes into account the experimentally established interactions among cancer cells, macrophages, free endothelial cells, MCP-1, VEGF and M-CSF. Simulations of the model predict the effect of

GM-CSF treatment on slowing tumor growth, and these predictions fit reasonably well with the *in vivo* experimental data of Eubank et al. (2008). Our hope is to incorporate modeling methods such as this to predict treatment success on various existing strategies in the clinical setting in terms of both the dosage and frequency of treatment. In fact, methods are currently being investigated to obtain more detailed information from the tumor microenvironment like tumor pH, intracellular glutathione, and redox potential that may affect existing chemotherapy drugs. Using these new data, better simulations could be generated for use in patients with breast cancer.

2. The model

We shall represent blood vessels in terms of the endothelial cells (EC) which line the interior of the capillaries. For simplicity we take the tumor to be a sphere and we denote its radius at time t by $R(t)$. The tumor region is defined by $0 \le r \le R(t)$ and the model's variables are given in Table 1.

We assume that these variables are radially symmetric, i.e., they depend only on r and t. It is also assumed that the macrophage density depends on the GM-CSF administration, in fact, GM-CSF induces macrophage chemotaxis (Ribatti et al., 2007).

The evolution of tumor cell density is given by

$$\frac{\partial c}{\partial t} = D_c \Delta c + \underbrace{\lambda_0(w)c}_{\text{necrosis}} + \underbrace{\lambda_1(w)c\left(1 - \frac{c+m+\delta b}{c^*}\right)}_{\text{proliferation}} - \underbrace{\mu_c C}_{\text{apoptosis}} . \tag{1}$$

The constant c^* represents the total capacity of tumor cells (live and dead) and macrophages competing for space, δ, are chosen such that $0 < \delta < 1$, since the volume of dead cells is smaller than the volume of live cells (Ward and King, 1997). The first term on the right-hand side accounts for the diffusion of tumor cells, the second term represents the fact that cells die at low oxygen concentrations at rate $\lambda_0(w)$ by necrosis, and the last term accounts for death due to apoptosis. Tumor cells are assumed to undergo a logistic growth and compete for space with macrophages and dead cells. The function $\lambda_1(w)$ is the growth rate of tumor cells. We assume that for oxygen concentration w in some range $w_n < w < w_1$ cells are in quiescent phase; and for $w > w_1$, the growth rate $\lambda_1(w)$ increases linearly in w, until it reaches a constant level when w crosses the hypoxic level w_h. The range $w_1 < w < w_h$ is considered to be in the hypoxic (but not extreme hypoxic) range, whereas the range $w > w_1$ is viewed as the normoxic range; one does not expect to have hyperoxic conditions within the tumor. Following (Breward et al., 2001), we choose $w_1 = 1.6 w_n$. Hence

$$\lambda_1(w) = \begin{cases} 0 & \text{if } w_n \le w \le w_1, \\ \dfrac{\lambda_1}{w_h - w_n}(w - w_1) & \text{if } w_1 < w \le w_h, \\ \lambda_1 & \text{if } w > w_h . \end{cases} \tag{2}$$

The rate of necrosis is assumed to occur at a faster rate than proliferation (Breward et al., 2001), and we take

$$\lambda_0(w) = -2\lambda_1 \frac{w_n - w}{w_n} \quad \text{if } w < w_n . \tag{3}$$

The evolution of dead tumor cell density is given by

$$\frac{\partial b}{\partial t} = D_b \Delta b \underbrace{-\lambda_0(w)c + \mu_c c}_{\text{gain from live tumor cells}} \underbrace{- \mu_b \frac{w}{w_0} mb}_{\text{clearance}}, \tag{4}$$

where w_0 is the oxygen density in normal tissue. The first term on the right-hand represents the dispersion of dead cells. The second and third terms account for the gain of dead cells due to death of tumor cells. Clearance of dead cells is driven by macrophages whose efficiency increases as the oxygen level increases.

The oxygen density evolves according to

$$\frac{\partial W}{\partial t} = D_w \Delta w + \underbrace{\lambda_2 e}_{O_2 \text{ delivered by EC}} - \underbrace{\lambda_3 wm}_{\text{uptake by macrophages}} - \underbrace{\lambda_4 wC}_{\text{uptake by tumor}} . \tag{5}$$

The first term in Eq. (5) accounts for the diffusion of oxygen and the second term accounts for the oxygen diffused from the vasculature. Oxygen is being taken up by both macrophages and tumor cells.

We view the vascular system as being represented by the density of the endothelial cells. The evolution of the endothelial cell density is given by

$$\frac{\partial e}{\partial t} = D_e \Delta e - \underbrace{\nabla \cdot (\kappa_h e \nabla h)}_{\text{chemotaxis}} + \underbrace{\lambda_5 e \left(1 - \frac{e}{e_1}\right)\left(\frac{h - h_1}{h_0}\right) H(h - h_1)}_{\text{proliferation}}, \tag{6}$$

where e_1 is the maximal EC density inside the tumor and it will be estimated later. The second term in the right-hand side of Eq. (6) accounts for the VEGF-dependent chemotactic movement of endothelial cells; we assume that the chemotactic coefficient κ_h is constant. Endothelial cells undergo a logistic type growth which is controlled by VEGF, and this is reflected by the third term in the right-hand side of Eq. (6). We assume that without the influence of VEGF, endothelial cells proliferation and apoptosis balance each other, so that net proliferation is due primarily to VEGF influence. We also assume that there is a threshold concentration level of VEGF below which proliferation does not occur (Acker et al., 2001; Seghezzi et al., 1998). This is expressed by the term $H(h-h_1)$, where $H(\cdot)$ is the Heaviside function. A similar term $\lambda_5 e(1-(e/e_0))((h-h_1)/h_0)H(h-h_1)$ was introduced in (Chaplain, 1995, p. 390 where e_0 accounts for the EC density in normal tissue; in our case, e_1 is the maximal EC density inside the tumor.

The density of the chemoattractant VEGF evolves according to

$$\frac{\partial h}{\partial t} = D_h \Delta h + \underbrace{\lambda_6(w)c + \lambda_7(w)\frac{s}{m+m_c}m}_{\text{secretion by tumor and macrophages}} - \underbrace{\lambda_8 g m h}_{\text{GM-CSF inhilition}} - \underbrace{\mu_h h}_{\text{decay}} . \tag{7}$$

The first and last terms in Eq. (7) account for diffusion and decay of VEGF. The second and third terms on the right-hand side account for the fact that VEGF is produced by both the tumor cells and macrophages triggered by M-CSF. The c-macrophage receptor that activates the signal transduction pathway which leads to VEGF (and MCP-1) expression in macrophages is responsible for the saturation effect in both VEGF and MCP-1 production by macrophages (Varney et al., 2005; Leonard et al., 1991; Curry et al., 2008; Eubank et al., 2003). The oxygen-dependent rates $\lambda_6(w)$ and $\lambda_7(w)$ are chosen as follow:

$$\lambda_6(w) = \begin{cases} 0 & \text{if } w < w_n, \\ \dfrac{4\lambda_6}{w_1 - w_n}(w - w_n) & \text{if } w_n \le w \le w_1, \\ 4\lambda_6 & \text{if } w_1 < w \le w_h, \\ \lambda_6 & \text{if } w > w_h \end{cases} \tag{8}$$

and

$$\lambda_7(w) = \begin{cases} 0 & \text{if } w < w_n, \\ \dfrac{2\lambda_7}{w_1 - w_n}(w - w_n) & \text{if } w_n \le w \le w_1, \\ 2\lambda_7 & \text{if } w_1 < w \le w_h, \\ \lambda_7 & \text{if } w > w_h \end{cases} . \tag{9}$$

Based on Lewis and Murdoch (2005), it is assumed here that VEGF production takes place only when w is above the necrotic level w_n, that this production rate increases with w, but falls off when w arises above the hypoxic level; more details are given in Section 2.8. The third term on the right-hand side of Eq. (7) accounts for the fact that GM-CSF stimulates macrophages to secrete soluble VEGF receptor which combines with VEGF and neutralizes it (Eubank et al., 2003).

M-CSF evolves according to

$$\frac{\partial S}{\partial t} = D_s \Delta s + \underbrace{\lambda_9 C}_{\text{secretion by tumor}} - \underbrace{\mu_s S}_{\text{decay}} , \tag{10}$$

where the first and last terms account for diffusion and decay, and the middle term accounts for the fact that M-CSF is produced by tumor cells (Leitzel et al., 2007). The parameter λ_9 is independent of the oxygen levels since the M-CSF promoter does not have HRE (hypoxia regulatory element), which senses low oxygen and responds by producing higher levels of the gene (Oren et al., 2001).

The equation for the macrophage density is

$$\frac{\partial m}{\partial t} = D_m \Delta m - \underbrace{\nabla \cdot \left(\kappa_p m \nabla p\right)}_{\text{chemotaxis by MCP-1}} - \underbrace{\nabla \cdot \left(\kappa_g m \nabla g\right)}_{\text{chemotaxis by GM-CSF}} . \tag{11}$$

The second and third terms account for their recruitment in response to chemoattractants MCP-1 and GM-CSF (Owen et al., 2004; DeVita et al., 2008, p. 2622). The chemotactic coefficients κ_p and κ_g are assumed to be constants.

MCP-1 is predominantly produced by macrophages and is a potent chemotactic factor for monocytes (Kanda et al., 2006). MCP-1 is produced in response to M-CSF binding the M-CSF receptor (Varney et al., 2005; Leonard et al., 1991; Curry et al., 2008; Eubank et al., 2003), a process that results in saturation due to limited M-CSF receptors. Hence, the MCP-1 equation is

$$\frac{\partial p}{\partial t} = D_p \Delta p + \underbrace{\lambda_{10}(w) \frac{s}{m + m_c} m}_{\text{secretion by macrophages}} - \underbrace{\mu_p p}_{\text{decay}} . \tag{12}$$

Hypoxia inhibits the production of MCP-1 from macrophages; the extent of inhibition ranging from 2.3- to 2.8-fold compared to normoxia (Bosco et al., 2004). Hence, we take

$$\lambda_{10}(w) = \begin{cases} 0 & \text{if } w < w_n, \\ \frac{2}{5}\lambda_{10} & \text{if } w_n \le w \le w_h, \\ \lambda_{10} & \text{if } w > w_h . \end{cases} \tag{13}$$

The GM-CSF equation is

$$\frac{\partial g}{\partial t} = D_g \Delta g + \underbrace{f(t)}_{\text{injection}} - \underbrace{\mu_g g}_{\text{decay}} , \tag{14}$$

where the second term $f(t)$ accounts for injecting GM-CSF periodically, depending on the dosing regimen.

2.1. Boundary conditions

Since the variables are radially symmetric, they all satisfy a no-flux condition at $r = 0, t > 0$. We assume that on the tumor boundary $r = R(t)$ the live tumor cell density is constant and that there are no dead cells. This assumption is justified since on the tumor boundary cells have a good supply of oxygen, so they do not undergo necrosis. All other variables (macrophages, EC, cytokines, oxygen) satisfy a Robin-type boundary condition

$$C\Big|_{r=R(t)} = c_0, \quad b\Big|_{r=R(t)} = 0,$$
$$\frac{\partial e}{\partial r} + \gamma_1 \Phi(h)\big(e - e_0\big)\Big|_{r=R(t)} = 0, \quad \frac{\partial m}{\partial r} + \gamma_1 \Gamma(p,g)\big(m - m_1\big)\Big|_{r=R(t)} = 0,$$
$$\Psi(e)\frac{\partial w}{\partial r} + \gamma_1\big(w - w_0\big)\Big|_{r=R(t)} = 0,$$
$$\frac{\partial s}{\partial r} + \gamma_2 s\Big|_{r=R(t)} = 0, \quad \frac{\partial p}{\partial r} + \gamma_2 p\Big|_{r=R(t)} = 0, \quad \frac{\partial h}{\partial r} + \gamma_2 h\Big|_{r=R(t)} = 0,$$
$$\frac{\partial g}{\partial r} + \gamma_2 g\Big|_{r=R(t)} = 0.$$

Here m_1 is the average macrophage density for the untreated tumor, as measured in Eubank et al. (2008), $\gamma_1\ \Phi(h)$ is the relative flux $(\partial e/\partial r)/(e_0 - e)$ of EC (similarly for macrophages and oxygen), γ_2 is the relative flux of the cytokines (s,p,h,g), and

$$\Phi(h) = \frac{h}{h + \alpha_1}, \quad \Gamma(p,g) = \frac{p}{p + \alpha_2} + \frac{g}{g + \alpha_3}, \quad \Psi(e) = \frac{\alpha_4}{e + \alpha_5},$$

where α_i, $i = 1,\ldots, 5$ are positive parameters. The form of the functions $\Phi(h), \Gamma(p,g), \Psi(e)$ represents the fact that the relative flux of EC, macrophages and oxygen increases with VEGF, MCP-1 and GM-CSF, and EC, respectively. Although we have assumed here a specific form for $\Phi(h), \Gamma(p,g), \Psi(e)$, the simulation results of our model do not significantly change if the form of these functions is not significantly altered.

2.2. Initial conditions

Palpable tumors had volume 1–2 mm^3 in Eubank et al. (2008). We take initial volume of 1 mm^3, which corresponds to initial radius $R_0 = 0.6$ mm. We also take the initial values

$$c(r,0) = c_0, \quad b(r,0) = 0, \quad w(r,0) = w_0, \quad e(r,0) = 0,$$
$$m(r,0) = m_1 e^{-\left(R_0 - x\right)/\epsilon},$$
$$h(r,0) = 0, \quad s(r,0) = 0, \quad p(r,0) = 0, \quad g(r,0) = 0 \quad \left(0 < r < R_0\right),$$

where $\epsilon > 0$.

2.3. Interface condition

We assume that live tumor and macrophage cells have the same volume, which is typically $V_L = 10^{-9}$ cm^3 (Ward and King, 1997). Cells that just died have the same volume as live cells, but shortly after they are degraded. Thus, on the average we view each volume of a dead cell as being a fraction of the volume of a live cell; we take it to be δV_L, where $\delta = 0.3$. Hence, the total volume occupied by the cells is

$$\left[\int_{r < R(t)} (m(r,t) + c(r,t) + \delta b(r,t))\right] \times 10^{-9} \text{ cell cm}^{-3}.$$

Since the cells occupy only a fraction θ of the total volume $V(t)$ of the tumor, where θ is a constant to be determined later on

$$\rho\theta V(t) = \int_{r < R(t)} (m(r,t) + c(r,t) + \delta b(r,t)) \quad \text{and} \quad \rho = 10^9 \text{ cell cm}^{-3}.$$

In order to determine how the tumor boundary $r = R(t)$ varies in time we differentiate the last equation with respect to t and use the boundary conditions for c and b

$$\rho\theta\frac{dV}{dt} = \frac{d}{dt}\int_{r < R(t)} (m(r,t) + c(r,t) + \delta b(r,t)) = \left(m(R(t),t) + c_0\right)\frac{dV}{dt} + \int_{r < R(t)} \frac{\partial}{\partial t}(m(r,t) + c(r,t) + \delta b(r,t)).$$

The integral term can be written as

$$\int_{r < R(t)} \frac{\partial}{\partial t}(m(r,t) + c(r,t) + \delta b(r,t)) = \Theta(c,b,m,p,g)\left(4\pi R^2\right) + \int_{r < R(t)} \left(\lambda_1(w)c\left(1 - \frac{c + m + \delta b}{c^*}\right) - \delta\mu_b\frac{w}{w_0}mb\right),$$

where

$$\Theta(c,b,m,p,g) = -\kappa_g m(R(t),t)\frac{\partial g}{\partial r}(R(t),t) - \kappa_p m(R(t),t)\frac{\partial p}{\partial r}(R(t),t) + D_m\frac{\partial m}{\partial r}(R(t),t) + D_c\frac{\partial C}{\partial r}(R(t),t) + \delta D_b\frac{\partial b}{\partial r}(R(t),t). \tag{15}$$

It follows that

$$\frac{dV}{dt}\left(\rho\theta - m(R(t),t) - c_0\right) = \Theta(c,b,m,p,g)\left(4\pi R^2\right) + \int_{r < R(t)} \left(\lambda_1(w)c\left(1 - \frac{c + m + \delta b}{c^*}\right) - \delta\mu_b\frac{w}{w_0}mb\right),$$

or, after dividing by $4\pi R^2$

$$\frac{dR}{dt} = \frac{\Theta(c,b,m,p,g)}{\rho\theta - m(R(t),t) - c_0} + \frac{\int_0^{R(t)} \left(\lambda 1(w)c\left(1 - \frac{c + m + \delta b}{c^*}\right) - \delta\mu_b\frac{w}{w_0}mb\right)r^2\,dr}{R^2\left(\rho\theta - m(R(t),t) - c_0\right)}. \tag{16}$$

2.4. Parameters

Table 2 lists the values of the parameters which appear in Eqs. (1)–(14) in dimensional and dimensionless forms. The last column gives reference to experimental data. When such data were not available, the parameters were estimated; some of these estimates are based on unpublished observations by co-authors Eubank and Roberts. The conversion from the dimensional to dimensionless units is done as follows:

$$\hat{r} = \frac{r}{L}, \quad \hat{t} = \frac{t}{\tau}, \quad \hat{C} = \frac{C}{C_0}, \quad \hat{b} = \frac{b}{c_0}, \quad \hat{e} = \frac{e}{e_0}, \quad \hat{m} = \frac{m}{m_0}, \quad \hat{C}^* = \frac{c^*}{c_0},$$

$$\hat{w} = \frac{w}{w_0}, \quad \hat{h} = \frac{h}{h_0}, \quad \hat{s} = \frac{s}{s_0}, \quad \hat{p} = \frac{p}{p_0}, \quad \hat{g} = \frac{g}{g_0}, \quad \hat{m}_c = \frac{m_c}{m_0},$$

$$\left\{\hat{D}_c, \hat{D}_b, \hat{D}_w, \hat{D}_e, \hat{D}_h, \hat{D}_m, \hat{D}_p, \hat{D}_g\right\} = \left\{D_c, D_b, D_w, D_e, D_h, D_s, D_m, D_p, D_g\right\}\frac{\tau}{L^2},$$

$$\left\{\hat{\lambda}_0(w), \hat{\lambda}_1(w), \hat{\lambda}_2, \hat{\lambda}_3, \hat{\lambda}_4, \hat{\lambda}_5\right\} = \tau\left\{\lambda_0(w), \lambda_1(w), \frac{e_0\lambda_2}{w_0}, \lambda_3 m_0, c_0\lambda_4, \lambda_5\right\}$$

$$\left\{\hat{\lambda}_6(w), \hat{\lambda}_7(w), \hat{\lambda}_8, \hat{\lambda}_9, \hat{\lambda}_{10}(w)\right\} = \tau\left\{\frac{c_0}{h_0}\lambda_6(w), \frac{m_0}{h_0}\lambda_7(w), \lambda_8 g_0 m_0, \frac{c_0}{s_0}\lambda_9, \frac{m_0\lambda_{10}}{p_0}\right\},$$

$$\left\{\hat{\kappa}_h, \hat{\kappa}_p, \hat{\kappa}_g\right\} = \left\{\kappa_h h_0, \kappa_p p_0, \kappa_g g_0\right\}\frac{\tau}{L^2},$$

$$\left\{\hat{\mu}_c, \hat{\mu}_b, \hat{\mu}_h, \hat{\mu}_s, \hat{\mu}_m, \hat{\mu}_p, \hat{\mu}_g\right\} = \left\{\mu_c, m_0\mu_b, \mu_h, \mu_s, \mu_m, \mu_p, \mu_g\right\}\tau,$$

$$\hat{m}_1 = \frac{m_1}{m_0}, \quad \hat{\alpha}_1 = \frac{\alpha_1}{h_0}, \quad \hat{\alpha}_2 = \frac{\alpha_2}{p_0}, \quad \hat{\alpha}_3 = \frac{\alpha_3}{g_0}, \quad \hat{\alpha}_{4,5} = \frac{\alpha_{4,5}}{e_0},$$

$$\hat{\gamma}_{1,2} = \gamma_{1,2}L, \quad \hat{\epsilon} = \frac{\epsilon}{L},$$

where the scaling parameters $L, \tau, e_0, s_0, p_0, g_0$ are given at the bottom of Table 2. We choose the length scale $L = 0.5$ cm and time scale $\tau = L^2/\max\{D_c, D_b, D_w, D_e, D_h, D_s, D_m, D_p\}$; then $\tau = 0.5\ \text{cm}^2/10^{-6}\ \text{cm}^2\ \text{s}^{-1} = 2.9$ days; this is comparable with the estimated tumor volume doubling time in Eubank et al. (2008), around 2.5 days.

2.5. Hypoxic/necrotic and VEGF threshold

The mean oxygen pressure in breast tumor patients is in the range of 3–15 mm Hg, while in normal breast tissue the mean oxygen pressure is substantially higher (52 mm Hg) in Vaupel et al. (2003). Accordingly, we take:

O_2 pressure in normal breast tissue is p_0=52 mm Hg,

maximal O_2 pressure in hypoxic region of tumor is $p_h = 12$ mm Hg,

maximal O_2 pressure in dead/necrotic region of tumor is $p_n = 3.75$ mm Hg.

The O_2 pressure in air is $p_a = 160$ mm Hg (Lane, 2002, p. 166). Since oxygen density is proportional to its pressure and O_2 density in air is $\rho_a = 1.43 \times 10^{-3}$ g cm^{-3} (Getman, 1908, p. 259), we obtain $w_0 = (p_0/p_a)\rho_a = 4.65 \times 10^{-4}$ g cm^{-3}, $w_h = (p_h/p_a)\,\rho_a = 1.07 \times 10^{-4}$ g cm^{-3} and $w_n = (p_n/p_a)\rho_a = 3.35 \times 10^{-5}$ g cm^{-3}.

The molecular weight of VEGF is 38 kDa (Frankel and Gillb, 2004). Hence, it can be shown that one molar of VEGF (1 M VEGF) is $\text{N}_\text{A} \times 38$ kDa × mol/l = 36.5 g cm^{-3}, where $N_\text{A} = 6 \times 10^{23}$ mol^{-1} is the Avogadro constant and 1 kDa = 1.66×10^{-27} kg is the unified atomic mass unit. The VEGF threshold h_1 below which proliferation does not occur, in Chaplain (1995), was chosen to be $h_1 \le 10^{-11}$ M. Qualitatively similar results have been obtained in Chaplain (1995) for $0 \le h_1 \le 4 \times 10^{-12}$ M. Based on these estimates, we take $h_1 = 10^{-11}$ M = 3.65×10^{-10} g cm^{-3}, but smaller values of h_1 do not qualitatively change our simulations.

2.6. Scaling parameters and volume fraction

It was observed in Eubank et al. (2008) that macrophages take up to 20% of the volume of the tumor. Hence, we take $m_0 = 2 \times 10^8$ cell cm^{-3}.

Extracellular volume fraction information was derived from magnetic resonance imaging in Vincensini et al. (2007) for malignant and benign lesions in breast tumors. For the malignant lesions [invasive ductal carcinomas (IDC) and invasive lobular carcinomas (ILC)] the extracellular volume fractions were in the range of 0.50 ± 0.32 and 0:30 ± 0.22, respectively. In this work we will assume that initially, tumor cells occupy 70% of the volume of the tumor and that, on the average, the combined volume fractions of macrophages and tumor cells is 90%. Hence, $\theta = \theta_c + \theta_m = 0.9$, where $\theta_c/\theta_m = c_0/m_0$.

To determine e_0 we assume that the average radius of the blood capillaries in normal tissue is 5 μm and parallel capillaries are 50 μm apart (Less et al., 1991). Then the density of the capillaries is $5^2/50^2 = 10^{-2}$ g cm^{-3}. Since EC occupy only a fraction of this volume, we estimate the EC volume fraction to weight $10^{-2}/4 = 2.5 \times 10^{-3}$ g cm^{-3} (Lewis and Murdoch, 2005, p. 27); it follows that the EC density is $e_0 = 2.5 \times 10^6$ cell/cm^{-3}. It has been shown in Less et al. (1991) that the mean capillary diameter in tumor is 10 μm, but the mean capillary distance in tumor is the same as in normal tissue. Based on this data we may assume that with angiogenesis, the maximal EC density inside the tumor e_1 is larger than in normal tissue, possibly by 2–3 times larger. We take $e_1 = 2e_0 = 5 \times 10^6$ cell cm^{-3}. Sottnik et al. (2010) have shown that the EC fraction in tumors in 0.335%. Our estimate of 0.5% is comparable with this value.

MCP-1 concentrations in the range of 0.2–6.3 ng ml^{-1} were reported in Owen and Sherratt (1997). M-CSF levels in breast tumors were measured in Ławicki et al. (2006), to be in the range of 134.5–1175.1 pg ml^{-1}, and VEGF levels in the range of 1–10 ng ml^{-1} were observed in Eubank et al. (2008). Hence (similarly to Schugart et al., 2008), we take $h_0 = 10$ ng ml^{-1} and choose the scaling parameters s_0, p_0, g_0 to be equal to h_0.

2.7. Proliferation and clearance/decay rates

Proliferation rates: Tumor cells have a usual doubling time 18–24 h (Owen et al., 2004). Hence we take the doubling time of 19 h, so that $\lambda_1 = (\ln 2/19)$ h$^{-1} = 10^{-5}$ s^{-1}. The proliferation rate of endothelial cells is 0.02–0.056 h^{-1} (Chaplain et al., 1995). Note that for small EC density e, the logistic term in Eq. (6) is approximately $\lambda_5 e(1-(e/e_1)) \approx 2\lambda_5 e$. We take $2\lambda_5 = 0{:}05$ h^{-1}, and hence, $\lambda_5 = 7 \times 10^{-6}$ s^{-1}.

Clearance/apoptosis rates: The proliferation rate of tumor cells is larger than the death rate by apoptosis; we take $\mu_c = \lambda_1/2 = 5 \times 10^{-6}$ s^{-1}. We assume that in the tumor periphery, the rate of clearance of dead cells (by macrophages; see Eq. (4)) is approximately the same as the rate of apoptosis of tumor cells, i.e., $\mu_b m_1 \approx \mu_c$, where m_1 is the macrophage density as measured in Eubank et al. (2008) (see the boundary condition for macrophages in Section 2.1). Since $m_1 = 10^8$ cell cm^{-3} (by Eubank et al., 2008), we get $\mu_b = 5 \times 10^{-14}$ cm^3 s^{-1} cell^{-1}.

Decay rates: The VEGF decay rate is $\mu_h = 0.456\ h^{-1}$, as in Plank et al. (2004). M-CSF is relatively stable, with a half-life of 3–4 h (Tang, 2000); hence, $\mu_s = (\ln 2/4)h^{-1} = 4.8 \times 10^{-5}\ s^{-1}$. The half-life of GM-CSF is between 10 and 14 h (Williams et al., 1999); we take $\mu_g = (\ln 2/12)\ h^{-1} = 1.6 \times 10^{-5}\ s^{-1}$. Finally, the MCP-1 decay rate is $\mu_p = 2 \times 10^{-5}\ s^{-1}$, as in Owen and Sherratt (1997).

2.8. Cytokine production rates

We will choose $\lambda_6, \lambda_7, \lambda_9, \lambda_{10}$ such that the corresponding dimensionless chemical production and decay rates are of the same order of magnitude (Owen and Sherratt, 1997).

VEGF production rate by tumor cells $\lambda_6(w)$ in (7) and (8): In Pyaskovskaya et al. (2008) the VEGF production rates were estimated for Lewis lung carcinoma in unfed culture over 5 days. VEGF production decreased from 35 to 5 pg/(10^6 cells × h), thus giving a range of $10^{-21} - 10^{20}$ g s^{-1} $cell^{-1}$. In Owen et al. (2004), the maximal production rate of a general chemoattractant (like VEGF and MCP-1) produced under hypoxia by tumor cells was taken to be $10^{-10} d_a$ M, where d_a is the decay rate of the chemical and 10^{-10} M is its typical concentration. We remark that our μ_h is smaller than the value of d_a in Owen et al. (2004) since VEGF is assumed to decay more rapidly. If the molar concentration of VEGF in the standard density units is 36.5 g cm^{-3} and we use the VEGF decay rate μ_h from Table 2, then the rate of VEGF production is 4.6×10^{-13} g cm^{-3} s^{-1}, and dividing by $c_0 = 7 \times 10^8$ cell cm^{-3} from Table 2 we obtain the rate 6.57×10^{-22} g s^{-1} $cell^{-1}$. Hence, we estimate the maximal VEGF production rate to be in the range of $6.57 \times 10^{-22} - 10^{-20}$ g s^{-1} $cell^{-1}$.

Studies have shown that the magnitude of induction of VEGF levels subjected to hypoxia varies with tissue type but generally falls between 2- and 4-fold. For example, 2–3-fold increase of VEGF in oral cell and lung carcinoma has been reported in Shang et al. (2006) and Koshikawa et al. (2003), 3–4-fold increase of VEGF in neuroblastoma (Rapella et al., 2002) and 2–4-fold increase of VEGF in overexpressed breast cancers in Braunstein et al. (2007). Hence, we take the maximal VEGF production rate in the hypoxic region to be four times larger than in the normoxic region and we choose $4\lambda_6 = 8.5 \times 10^{-22}$ g s^{-1} $cell^{-1}$ to be consistent with the estimated range of VEGF production rates.

VEGF production rate by macrophages $\lambda_7(w)$ in (7) and (9): Hypoxia is a stimulus for the VEGF expression in human monocytes, inducing up to 5-fold increase in the levels of VEGF (Melillo et al., 1999). VEGF production is also unregulated from macrophages when treated with M-CSF (Curry et al., 2008), about 2-fold compared to the unstimulated sample. The amount of VEGF secreted by macrophages is at least 2–3 times the amount secreted by tumor cells (Vicioso et al., 2006). Although VEGF levels by both tumor cells and macrophages are elevated during hypoxia, it is not clear as to which cell type produces more VEGF in the hypoxic regions. Based on Vicioso et al. (2006), we assume that in the normoxic region ($w > w_h$) the proportion of VEGF produced by macrophages and tumor cells is approximately 2.1, i.e., $\lambda_7 m_0 = 2\lambda_6 c_0$, but in the hypoxic region ($w_1 < w < w_h$) it is approximately 1.1, i.e., $2\lambda_7 m_0 = 4\lambda_6 c_0$.

M-CSF production rate by tumor cells λ_9 in (10): We compare the M-CSF production rate by tumor cells, λ_9, to the production rate, $\lambda_6(w)$, of VEGF. The mRNA levels for VEGF and M-CSF from osteoclast differ in hypoxic and normoxic conditions; at normal oxygen levels M-CSF production is higher than VEGF and at low oxygen levels VEGF production is higher than M-CSF in Utting et al. (2010). In the absence of relevant studies for tumors that would compare M-CSF and VEGF production in normoxia, we assume that the same comparison holds for tumor cells, and take $\lambda_9 = 1.5\lambda_6$.

MCP-1 production rate by macrophages $\lambda_{10}(w)$ in (12) and (13): We take the normoxic basal level of MCP-1 production to be the same as the VEGF production by macrophages, i.e., $\lambda_{10} = \lambda_7$. Since hypoxia inhibits the production of MCP-1 from macrophages about 2.5-fold compared to normoxia (Bosco et al., 2004), we take the MCP-1 production under hypoxic conditions to be $2/5\lambda_{10}$.

2.9. Chemotactic, diffusion/dispersion and oxygen uptake/delivery rates

Chemotactic coefficients: Similar to Section 2.5, where the molar concentration of VEGF (36.5 g cm^{-3}) was shown, taking 10 kDa as the molecular weight of MCP-1 and 22 kDa as the molecular weight of GM-CSF, we obtain that the molar concentration of MCP-1 and GM-CSF is 10 g cm^{-3} and 22 g cm^{-3}, respectively. The chemotactic coefficient for MCP-1 is in the range of 20–60 $cm^2\ s^{-1}\ M^{-1}$ (Schugart et al., 2008; Owen et al., 2004) and we take $\kappa_p = 60\ cm^2\ s^{-1}\ M^{-1}$. The chemotactic coefficient for VEGF is $\kappa_h = 36.5\ cm^2\ s^{-1}\ M^{-1}$, as in Schugart et al. (2008). In the absence of chemotactic data for GM-CSF, we assume κ_g to be comparable with κ_h, κ_p and take $\kappa_g = 20\ cm^2\ s^{-1}\ M^{-1}$. The molar concentrations of VEGF, MCP-1 and GM-CSF allow us to write $\kappa_h, \kappa_p, \kappa_g$ in the equivalent units $cm^5\ g^{-1}\ s^{-1}$ in Table 2.

Oxygen consumption rates: Oxygen consumption rates in murine macrophage-like RAW264.7 cells were measured in Nalwaya and Deen (2008) to be 32 ± 3 pmol/(10^6 cells × s), typical of mammalian cells. Since the molar volume of oxygen is approximately 22.4 l/mol, this gives a range for λ_3 of 6.5 – 7.8 × $10^{-13}\ cm^3\ s^{-1}\ cell^{-1}$ and we choose $\lambda_3 = 7 \times 10^{-13}\ cm^3\ s^{-1}\ cell^{-1}$. In Girgis-Gabardo and Hassell (2008) the oxygen consumption rate by tumor cells was estimated to be $2.78 \times 10^{-17}\ mol\ cell^{-1}\ s^{-1}$, thus giving a rate of $6.2 \times 10^{-13}\ cm^3\ s^{-1}\ cell^{-1}$. However, older tumors harvested for 13–15 days showed smaller oxygen uptake rates in Butterworth and Cater (1967), even 50% smaller on day 15. Taking into account the Warburg effect (Chen et al., 2009), we assume that the total oxygen uptake by tumors cells is larger than by macrophages, possibly 2-fold larger. Hence, we take $\lambda_4 = 2\lambda_3 m_0/c_0 = 4 \times 10^{-13}\ cm^3\ s^{-1}\ cell^{-1}$.

Oxygen delivery rates: Since the oxygen level in tumor decreases as the tumor grows, the oxygen delivery by EC, $\lambda_2 e$, is smaller than the oxygen consumed (primarily by tumor cells), so that $\lambda_2 e < \lambda_4 wc$, or, $\lambda_2 < \lambda_4[wc/e]_{\text{average}}$. We take $\lambda_2 = c_0 w_0\ \lambda_4/(75e_0)$.

Diffusion/dispersion rates: The diffusion rates D_c, D_m, D_w and the dispersion rate D_b are based on the values in the references from Table 2. Diffusion of endothelial cells is in the range of $10^{-12} - 10^{-10}\ cm^2\ s^{-1}$ (Owen et al., 2004; Plank et al., 2004) and we take $D_e =$

10^{-11} cm^2 s^{-1}. In Owen et al. (2004) and Owen and Sherratt (1997) the diffusion rate of MCP-1 was 2×10^{-6} cm^2 s^{-1}; we take it to be $D_p = 10^{-6}$ cm^2 s^{-1}. We assume that the diffusion rates of VEGF, M-CSF and GM-CSF are similar.

2.10. Sensitivity analysis

In the model developed in this paper there are a number of parameters which are estimated and may affect significantly the simulation results. We have chosen to test the following parameters: θ_c, D_b, w_1, λ_9, γ_2, λ_4, θ_m, λ_1, γ_1, c^*. Although $\theta_c, \theta_m, \lambda_1$ have experimentally known ranges, these parameters have been included here, since they play an important role in our model. In order to see how sensitive the tumor radius is to these parameters (at days 3, 14 and 21), we have performed sensitivity analysis. We have chosen a range for each of these parameters and used Latin hypercube sampling to generate 200 samples. (The range of the tested parameters is given in Table 3, all other parameters are as in Table 2.) For each of the 10 parameters a partial rank correlation coefficient (PRCC) is calculated, the sign of which determines whether an increase in the parameter value will increase or decrease the tumor radius at a given time. The sensitivity analysis was carried out based on the method in Marino et al. (2008) and using the Matlab files available at http://malthus.micro.med.umich.edu/lab/usadata/.

Out of the 10 parameters tested eight were statistically significant (p-value < 0.01) at day 14 (θ_c, w_1, γ_2, λ_4, θ_m, λ_1, γ_1, c^*), seven at day 21 (θ_c, w_1, λ_4, θ_m, λ_1, γ_1, c^*) and only five at day 3 (θ_c, D_b, θ_m, λ_1, c^*). Fig. 1 shows the statistically significant PRCC values (p-value < 0.01) of the parameters of interest for $R(t)$ at days 3, 14 and 21. We conclude that the tumor radius at days 14 and 21 is positively correlated to the parameters $\theta_c, \lambda_1, \gamma_1, c^*$ and negatively correlated to w_1, λ_4, θ_m. In particular, $R(t)$ increases if θ_c/θ_m increases and if the proliferation rate λ_1 increases.

3. Results

All simulations were carried out with MATLAB (version R2009a Mathworks). The model equations were numerically solved using pdepe (MATLAB function for initial-boundary value problems for parabolic-elliptic PDEs in 1D) in each time step. The ODE for the interface condition was calculated using an explicit second-order Runge–Kutta method.

The spatial distribution of tumor cells (live and dead) and macrophages at days 7 and 14 are shown in Fig. 2(a) and (b). The density of live tumor cells increases toward the rim of the tumor, where there is more oxygen supply, whereas the density of the dead cell increases toward the center of the tumor where hypoxic conditions hold. Fig. 2(c) illustrates the evolution of the average tumor (live and dead) and macrophage densities over 21 days. Since most live tumor cells are near the rim, where the level of oxygen is high enough to keep them live and proliferating, the average density of these cell taken over the entire tumor decreases as the tumor increases; the reverse holds for the dead cells.

Fig. 3 shows the simulation results in two cases; no GM-CSF is given (the solid line) and 100 ng of GM-CSF administered three times a week: Monday, Wednesday and Friday (the dashed line). Experimental data from Eubank et al. (2008) in both cases are indicated by

circles. The simulations fit well with the experimental data from Pollard (1997) in both cases. Indeed, the statistical precision of fit by the model was confirmed by a strong correlation coefficient between the experimental data and the simulation results (0.99 for the untreated and 0.988 for the GM-CSF treated case).

Fig. 4(a) simulates the tumor volume growth for different doses of GM-CSF (10, 50 and 100 ng) injected three times a week in equal volume. The 100 ng dose results in a 93.4% volume reduction compared to the volume of the untreated tumor. These results seem predictable as the highest dose of GM-CSF (100 ng) was most effective in tumor growth inhibition. It is interesting that this effect reaches a plateau as 10-fold more GM-CSF showed little effect on tumor growth *in vivo* (unpublished observation by coauthors Eubank and Roberts) driven by augmented receptor down-regulation on the macrophages. The average density of EC for the different doses of GM-CSF is shown in Fig. 4(b). Experimental data from Eubank et al. (2008) predict that the mean value of the average EC density at day 21 for the tumor treated by 100 ng of GM-CSF is 82% less than the mean value of the average EC density of the untreated tumor, while our model predicts a decrease in EC density by 89.8% at day 21 compared to the EC density of the untreated tumor for GM-CSF. This discrepancy may be attributed to several factors such as: (i) GM-CSF was not evenly distributed throughout the tumor, or (ii) the predicted half-life of GM-CSF is longer than 12 h.

Fig. 4(c) predicts macrophage density fluctuations which are GM-CSF dependent. At large doses of GM-CSF (100 ng per injection three times a week) the GM-CSF gradient in Eq. (11) becomes large and, as GM-CSF cleares up in 1–2 days, macrophage chemotaxis slows down. Experimental data from Eubank et al. (2008) show increased macrophage recruitment into the tumors after 21 days, but our model predicts a “fluctuating” migration of macrophages within the tumor treated by GM-CSF. We speculate that the fluctuation in macrophage density may arise from recruitment of macrophage precursor cells (monocytes) from the bone marrow upon GM-CSF injection into the tumor. GM-CSF is a known recruiter of white blood cells and has been used clinically to increase these cell numbers to help patients recover after bone marrow transplant.

Further, *in vivo* data suggest that the above macrophages are of an M1, tumor-fighting phenotype while macrophages in the PBS-treated tumors represent more of a tumor-helping, M2 phenotype (Eubank et al., 2008). This observation is intriguing because the presence of tumor macrophages in breast cancer patients predict poor prognosis (Lin and Pollard, 2004). Lin and Pollard (2004) have shown that the absence of TAMs did not change the incidence or growth of the primary tumor but decreased its rate of progression and inhibited metastasis. This is contrary to the finding in Eubank et al. (2008) which suggests that increases in tumor macrophage numbers in the presence of GM-CSF increases survival.

Our model can be used to evaluate the efficacy of different dosing protocols, while keeping the total amount of GM-CSF injected the same in the three week period (900 ng). Fig. 5 compares breast tumor growth from the following protocols: once a week (300 ng each Monday), twice week (150 ng each Monday and Thursday), three times a week (100 ng each Monday, Wednesday, and Friday), or daily (42.8 ng each day). Interestingly, our model predicts that when the total amount of GM-CSF delivered to the tumor is fixed (900 ng), a

more frequent treatment is more effective. This ability to predict the effect of dosing schedules in therapy may help alleviate factors such as toxicity to the patients. For example, if higher doses of GM-CSF are not well tolerated, the dosage could be reduced and administered more frequently. Our model predicts that, with the half-life of GM-CSF at 12 h, changing treatment from a high dose of 300 ng once a week to 150 ng twice a week can reduce tumor growth by a factor of 3.66 after 3 weeks. We speculate that this improvement hinges mostly on the timed influx of macrophages and on the half-life of GM-CSF.

4. Conclusion

M-CSF is over-expressed in most human breast cancers and triggers macrophages to produce biologically-active VEGF and MCP-1. MCP-1 attracts monocytes into the tumor which, in turn, differentiate into tumor-associated macrophages (TAMs). Thus, MCP-1 indirectly enhances the production of VEGF by TAM recruitment. TAMs have been shown to produce factors like MMPs and VEGF to induce new capillary formation from nearby blood vessels—feeding the tumor and enabling it to grow. The growth factor GM-CSF blocks the proliferative activity of VEGF on endothelial cells by stimulating mononuclear phagocytes to secrete soluble VEGF receptor-1 which sequesters VEGF and inhibits binding to its cognate receptors, VEGFR-1 and −2. Hence, GM-CSF may be considered as a potential therapy to block angiogenesis, thereby inhibiting tumor growth. Indeed, GM-CSF in combination with Herceptin is currently in phase II clinical study for treatment of invasive breast carcinoma (Herceptin and GM-CSF for metastatic breast cancer, M.D. Anderson Cancer Center, last updated 30 September 2010).

In this work, we develop a mathematical model which predicts the anti-angiogenic activity of GM-CSF. The model simulations correlate with experimental results for the PyMT mouse model of breast cancer. This work demonstrates the potential of mathematical modeling as a tool to generate hypotheses for successful treatment strategies of solid tumors. In this setting, our modeling predicts optimal dosing and administration scheduling of GM-CSF. Such information can be used to limit treatment toxicity for the patient. Studies are underway to validate this observation experimentally.

The model developed in this paper is based on interactions among several important variables which are involved in GM-CSF treatment of breast cancer in mice. This model could be further refined by including, more explicitly, interactions between macrophages and other immune cells like T cells, or other microenvironment elements like fibroblasts, or cytokines that drive a malignant transition. Observations learned from this study are already being utilized in the laboratory (by coauthor Eubank) to enhance treatment of human breast cancer in immunodeficient mice. Further, novel delivery methods for GM-CSF are being developed to limit the need for direct injections at the tumor site. For example, tests using GM-CSF-containing nanospheres which target macrophages are underway. Successful completion of these studies will pave the way for moving GM-CSF into human clinical trials for breast cancer.

Acknowledgements

The research leading to these results has been supported by the National Science Foundation under Grant agreement no. DMS0931642 and by the National Cancer Institute Grant no. K99 CA131552–01.

References

Acker T, Beck H, Plate KH, 2001 Cell type specific expression of vascular endothelial growth factor and angiopoietin-1 and −2 suggests an important role of astrocytes in cerebellar vascularization. Mech. Dev 108, 45–57. [PubMed: 11578860]

Armstrong CA, Botella R, Galloway TH, et al., 1996 Antitumor effects of granulocyte macrophage colony stimulating factor production by melanoma cells. Cancer Res. 56, 2191–2198. [PubMed: 8616871]

Baj-Krzyworzeka M, Szatanek R, Weglarczyk K, Baran J, Zembala M, 2007 Tumour-derived microvesicles modulate biological activity of human monocytes. Immunol. Lett 113 (2), 76–82. [PubMed: 17825925]

Bosco MC, Puppo M, Pastorino S, Mi Z, Melillo G, Massazza S, Rapisarda A, Varesio L, 2004 Hypoxia selectively inhibits monocyte chemoattractant protein-1 production by macrophages. J. Immunol 172 (3), 1681–1690. [PubMed: 14734750]

Braunstein S, Karpisheva K, Pola C, Goldberg J, Hochman T, Yee H, Cangiarella J, Arju R, Formenti SC, Schneider RJ, 2007 A hypoxia-controlled cap-dependent to cap-independent translation switch in breast cancer. Mol. Cell 28, 501–512. [PubMed: 17996713]

Breward CJW, Byrne HM, Lewis CE, 2001 Modelling the interactions between tumour cells and a blood vessel in a microenvironment within a vascular tumour. Eur. J. Appl. Math 12, 529–556.

Butterworth AE, Cater DB, 1967 Effect of lysolecithin on the oxygen uptake of tumour cells, polymorphonuclear leucocytes, lymphocytes and macrophages in vitro. Br. J. Cancer 21 (2), 373–389. [PubMed: 4291113]

Caldwell J, Locey B, Clarke MF, Emerson SG, et al., 1991 Influence of medium exchange schedules on metabolic growth, and GM-CSF secretion rates of genetically engineered NIH-3T3 cells. Biotechnol. Prog 7 (1), 1–8. [PubMed: 1366977]

Chaplain MAJ, Giles SM, Sleeman BD, Jarvis RJ, 1995 A mathematical analysis of a model for tumour angiogenesis. J. Math. Biol 33, 744–770. [PubMed: 7561535]

Chaplain MAJ, 1995 The mathematical modeling of tumour angiogenesis and invasion. Acta Biotheoret. 43, 387–402.

Chen Y, Cairns R, Papandreou I, Koong A, Denko NC, 2009 Oxygen consumption can regulate the growth of tumors, a new perspective on the warburg effect. PLOS One 4 (9), e7033. [PubMed: 19753307]

Curry JM, Eubank TD, Roberts RD, Wang Y, Pore N, Maity A, Marsh CB, 2008 M-CSF signals through the MAPK/ERK pathway via Sp1 to induce VEGF production and induces angiogenesis in vivo. PLoS One 3 (10), e3405. [PubMed: 18852899]

DeVita VT, Lawrence TS, Rosenberg SA, Weinberg RA, DePinho RA, 2008 DeVita, Hellman, and Rosenberg's Cancer: Principles and Practice of Oncology. Lippincott Williams and Wilkins.

Eubank T, Roberts RD, Khan M, Curry JM, et al., 2008 GM-CSF inhibits breast cancer growth and metastases by invoking an anti-angiogenic program in tumor-educated macrophages. Cancer Res. 69 (5), 2133–2140.

Eubank TD, Galloway M, Montague CM, Waldman WJ, Marsh CB, 2003 M-CSF induces vascular endothelial growth factor production and angiogenic activity from human monocytes. J. Immunol 171 (5), 2637–2643. [PubMed: 12928417]

Eubank TD, Roberts R, Galloway M, Wang Y, et al., 2004 GM-CSF induces expression of soluble VEGF receptor 1 from human monocytes and inhibits angiogenesis in mice. Immunity 21, 831–842. [PubMed: 15589171]

Frankel AE, Gillb PS, 2004 VEGF and myeloid leukemias. Leukemia Res. 28 (7), 675–677. [PubMed: 15158088]

Fujimoto H, Sangai T, Ishii G, Ikehara A, Nagashima T, Miyazaki M, Ochiai A, 2009 Stromal MCP-1 in mammary tumors induces tumor-associated macrophage infiltration and contributes to tumor progression. Int. J. Cancer 125 (6), 1276–1284. [PubMed: 19479998]

Girgis-Gabardo A, Hassell JA, 2008 Scale-up of breast cancer stem cell aggregate cultures to suspension bioreactors. Biotechnol. Prog 22, 801–810.

Getman FH, 1908 Laboratory Exercises in Physical Chemistry. John Wiley & Sons, New York.

Gordon S, 2003 Alternative activation of macrophages. Nat. Rev. Immunol 3 (1), 23–35. [PubMed: 12511873]

Hagemann T, Robinson SC, Schulz M, Trümper L, et al., 2004 Enhanced invasiveness of breast cancer cell lines upon co-cultivation with macrophages is due to TNF-alpha dependent up-regulation of matrix metalloproteases. Carcinogenesis 25, 1543–1549. [PubMed: 15044327]

Hashizume H, et al., 2000 Openings between defective endothelial cells explain tumor vessel leakiness. Am. J. Pathol 156 (4), 1363–1380. [PubMed: 10751361]

Kanda H, Tateya S, Tamori Y, Kotani K, Hiasa K, Kitazawa R, Kitazawa S, Miyachi H, Maeda S, Egashira K, Kasuga M, 2006 MCP-1 contributes to macrophage infiltration into adipose tissue, insulin resistance, and hepatic steatosis in obesity. J. Clin. Invest 116 (6), 1494–1505. [PubMed: 16691291]

Kelly CE, Leek RD, Byrne HM, Cox SM, Harris AL, Lewis CE, 2002 Modelling macrophage infiltration into avascular tumours. J. Theoret. Med 4 (1), 21–38.

Koshikawa N, Iyozumi A, Gassmann M, Takenaga K, 2003 Constitutive upregulation of hypoxia-inducible factor-1a mRNA occurring in highly metastatic lung carcinoma cells leads to vascular endothelial growth factor overexpression upon hypoxic exposure. Oncogene 22, 6717–6724. [PubMed: 14555985]

Lane N, 2002 Oxygen: The Molecule that Made the World. Oxford University Press.

Ławicki S, Szmitkowski M, Wojtukiewicz M, 2006 The pretreatment plasma level and diagnostic utility of M-CSF in benign breast tumor and breast cancer patients. Clin. Chim. Acta 371, 112–116. [PubMed: 16631152]

Leitzel K, Ettenberg S, Walsh R, Abraham J, Modur V, Braendle E, Evans DB, Ali SM, Demers L, Lipton A, 2007 Elevated serum M-CSF level predicts reduced survival in metastatic breast cancer patients. Journal of Clinical Oncology, ASCO Annual Meeting Proceedings I, vol. 25(18S).

Leonard EJ, Skeel A, Yoshimura T, Rankin J, 1991 Adv. Exp. Med. Biol 351, 55–64.

Less JR, Skalak TC, Sevick EM, Jain RK, 1991 Microvascular architecture in a mammary carcinoma: branching patterns and vessel dimensions. Cancer Res. 51, 265–273. [PubMed: 1988088]

Levine HA, Nilsen-Hamilton M, 2006 Angiogenesis—a biochemical/mathematical prospective In: Friedman A (Ed.), Springer Lecture Notes in Mathematics. Tutorials in Mathematical Biosciences III, vol. 1872; 2006.

Lewis C, Murdoch C, 2005 Macrophage responses to hypoxia. Am. J. Pathol 167 (3), 627–635. [PubMed: 16127144]

Lin EY, Nguyen AV, Russell RG, Pollard JW, 2001 Colony stimulating factor 1 promotes progression of mammary tumors to malignancy. J. Exp. Med 193, 727–740. [PubMed: 11257139]

Lin EY, Pollard JW, 2004 Macrophages: modulators of breast cancer progression. Novartis Found. Symp 256, 158–168. [PubMed: 15027489]

Mantovani A, Sica A, Locati M, 2007 New vistas on macrophage differentiation and activation. Eur. J. Immunol 37 (1), 14–16. [PubMed: 17183610]

Mantovani A, Sica A, Locati M, 2005 Macrophage polarization comes of age. Immunity 23 (4), 344–346. [PubMed: 16226499]

Mantovani A, Sozzani S, Locati M, Allavena P, Sica A, 2002 Macrophage polarization: tumor-associated macrophages as a paradigm for polarized M2 mononuclear phagocytes. Trends Immunol. 23 (11), 549–555. [PubMed: 12401408]

Marino S, Hogue IB, Ray Ch.J., Kirschner DE, 2008 A methodology for performing global uncertainty and sensitivity analysis in systems biology. J. Theoret. Biol 254, 178–196. [PubMed: 18572196]

Melillo G, Sausville EA, Cloud K, Lahusen T, Varesio L, Senderowicz AM, 1999 Flavopiridol, a protein kinase inhibitor, down-regulates hypoxic induction of vascular endothelial growth factor expression in human monocytes. Cancer Res. 59, 5433–5437. [PubMed: 10554012]

Nalwaya N, Deen WM, 2008 Nitric oxide, oxygen, and superoxide formation and consumption in macrophage cultures. Chem. Res. Toxicol 18, 486–493.

Oren H, Duman N, Abacioglu H, Ozkan H, Irken G, 2001 Association between serum macrophage colony-stimulating factor levels and monocyte and thrombocyte counts in healthy, hypoxic, and septic term neonates. Pediatrics 108 (2), 329–332. [PubMed: 11483796]

Owen MR, Byrne HM, Lewis CE, 2004 Mathematical modelling of the use of macrophages as vehicles for drug delivery to hypoxic tumour sites. J. Theoret. Biol 226, 377–391. [PubMed: 14759644]

Owen MR, Sherratt JA, 1997 Pattern formation and spatiotemporal irregularity in a model for macrophage–tumor interactions. J. Theoret. Biol 189, 63–80. [PubMed: 9398504]

Plank MJ, Sleeman BD, Jones PF, 2004 A mathematical model of tumour angiogenesis, regulated by vascular endothelial growth factor and the angiopoietins. J. Theoret. Biol 229, 435–454. [PubMed: 15246783]

Pollard JW, 1997 Role of colony stimulating factor-1 in reproduction and development. Mol. Reprod. Dev 46 (54).

Pyaskovskaya ON, Kolesnik DL, Kolobov AV, Vovyanko SI, Solyanik GI, 2008 Analysis of growth kinetics and proliferative heterogeneity of Lewis lung carcinoma cells growing as unfed culture. Exp. Oncol 30 (4), 269–275. [PubMed: 19112423]

Qian B, Deng Y, Im JH, Muschel RJ, Zou Y, Li J, Lang RA, Pollard JW, 2009 A distinct macrophage population mediates metastatic breast cancer cell extravasation. Establishment and growth. PLOS One 4 (8), e6562. [PubMed: 19668347]

Rapella A, Negrioli A, Melillo G, Pastorino S, Varesio L, Bosco MC, 2002 Flavopirisol inhibits vascular endothelial growth factor production induced by hypoxia or picolinic acid in human neuroblastoma. Int. J. Cancer 99, 658–664. [PubMed: 12115498]

Ribatti D, Nico B, Crivellato E, Vacca A, 2007 Macrophages and tumor angiogenesis. Leukemia 21, 2085–2089. [PubMed: 17878921]

Sapi E, 2004 The role of CSF-1 in normal physiology of mammary gland and breast cancer: an update. Exp. Biol. Med. (Maywood.) 229, 1–11. [PubMed: 14709771]

Shang Z-J, Li Z-B, Li J-R, 2006 VEGF is up-regulated by hypoxic stimulation and related to tumour angiogenesis and severity of disease in oral squamous cell carcinoma: in vitro and in vivo studies. Int. J. Oral Maxillofac. Surg 35, 533–538. [PubMed: 16388929]

Schugart R, Friedman A, Zhao R, Sen CK, 2008 Wound angiogenesis as a function of tissue oxygen tension: a mathematical model. Proc. Natl. Acad. Sci 105 (7), 2628–2633. [PubMed: 18272493]

Seghezzi G, Patel S, Ren CJ, Gualandris A, Pintucci G, Robbins ES, Shapiro RL, Galloway AC, Rifkin DB, Mignatti P, 1998 Fibroblast growth factor-2 (FGF-2) induces vascular endothelial growth factor (VEGF) expression in the endothelial cells of forming capillaries: an autocrine mechanism contributing to angiogenesis. J. Cell Biol 141 (7), 1659–1673. [PubMed: 9647657]

Sottnik JL, Guth AM, Mitchell LA, Dow SW, 2010 Minimally invasive assessment of tumor angiogenesis by fine needle aspiration and flow cytometry. Angiogenesis 13 (3), 251–258. [PubMed: 20734228]

Tang R, Beuvon F, Ojeda M, Mosseri V, et al., 1992 M-CSF (monocyte colony stimulating factor) and M-CSF receptor expression by breast tumour cells: M-CSF mediated recruitment of tumour infiltrating monocytes. J. Cell. Biochem 50, 350–356. [PubMed: 1334964]

Tang S, et al., 2000 Internalization and half-life of membrane-bound macrophage colony-stimulating factor. Chin. Sci. Bull 45 (18), 1697–1703.

Utting JC, Flanagan AM, Brandao-Burch A, Orriss IR, Arnett TR, 2010 Hypoxia stimulates osteoclast formation from human peripheral blood. Cell Biochem. Funct 28 (5), 374–380. [PubMed: 20556743]

Varney ML, Olsen KJ, Mosley RL, Singh RK, 2005 Paracrine regulation of vascular endothelial growth factor—a expression during macrophage–melanoma cell interaction: role of monocyte

chemotactic protein-1 and macrophage colony-stimulating factor. J. Interferon Cytokine Res 25 (11), 674–683. [PubMed: 16318581]

Vaupel P, Mayer A, Briest S, Höckel M, 2003 Oxygenation gain factor: a novel parameter characterizing the association between hemoglobin level and the oxygenation status of breast cancers. Cancer Res. 63, 7634–7637. [PubMed: 14633681]

Vincensini D, Dedieub V, Eliat PA, Vincent C, Bailly C, de Certainese J, Joffref F, 2007 Magnetic resonance imaging measurements of vascular permeability and extracellular volume fraction of breast tumors by dynamic Gd-DTPA-enhanced relaxometry. Magn. Reson. Imaging 25, 293–302. [PubMed: 17371717]

Vicioso L, Gonzalez FJ, Alvarez M, Ribelles N, Molina M, Marquez A, Perez L, Matilla A, Alba E, 2006 Elevated serum levels of vascular endothelial growth factor are associated with tumor-associated macrophages in primary breast cancer. Am. J. Clin. Pathol 125, 111–118. [PubMed: 16482999]

Ward JP, King JR, 1997 Mathematical modeling of avascular tumor growth. IMA J. Math. Appl. Med. Biol 14, 39–69. [PubMed: 9080687]

Williams MA, Kelsey SM, Newland AC, 1999 GM-CSF and stimulation of monocyte/macrophage function *in vivo* relevance and *in vitro* observations. Eur. J. Cancer 35 (3), S1–S22.

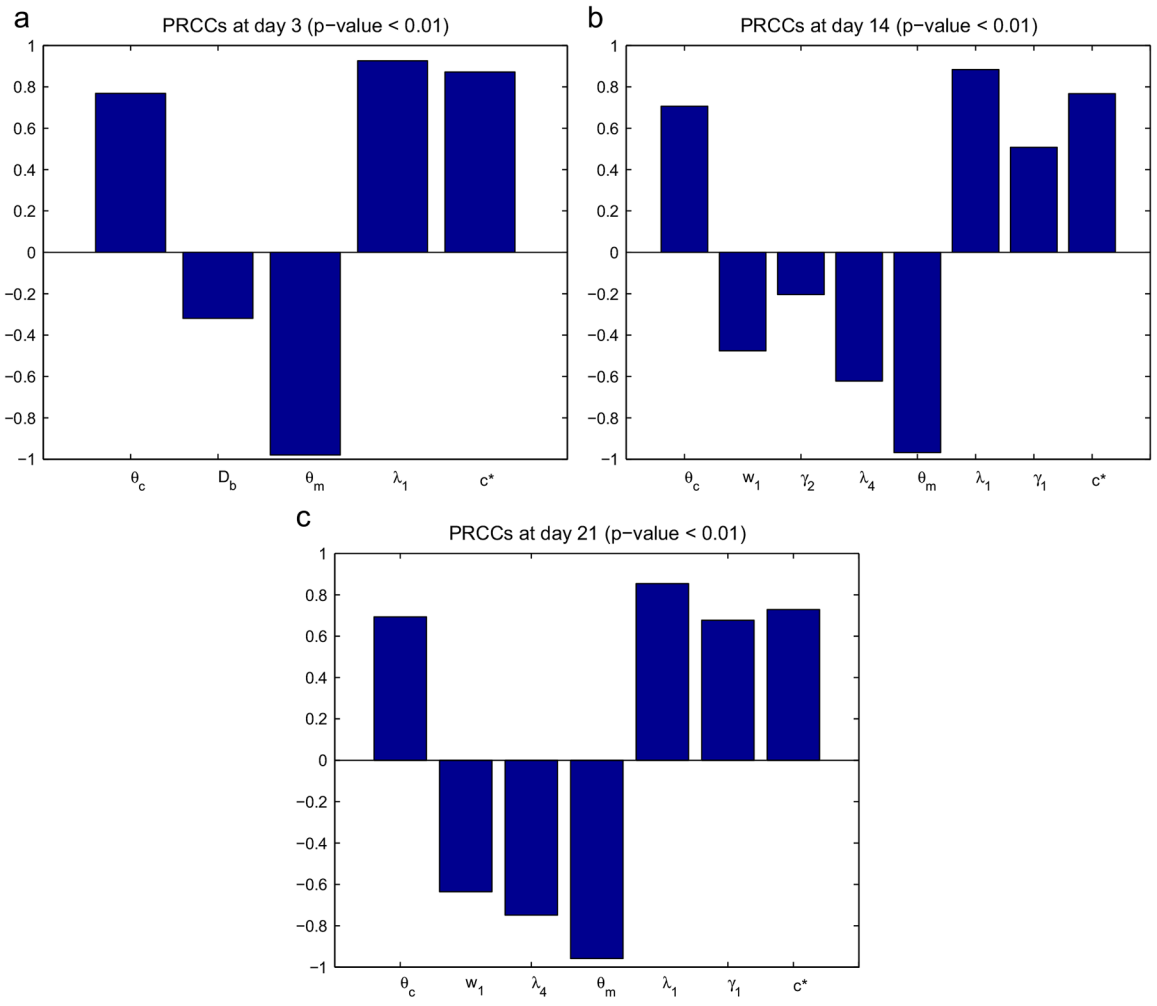

Fig. 1.

Statistically significant PRCC values (p-value < 0.01) for $R(t)$ at (a) day 3, (b) day 14 and (c) day 21.

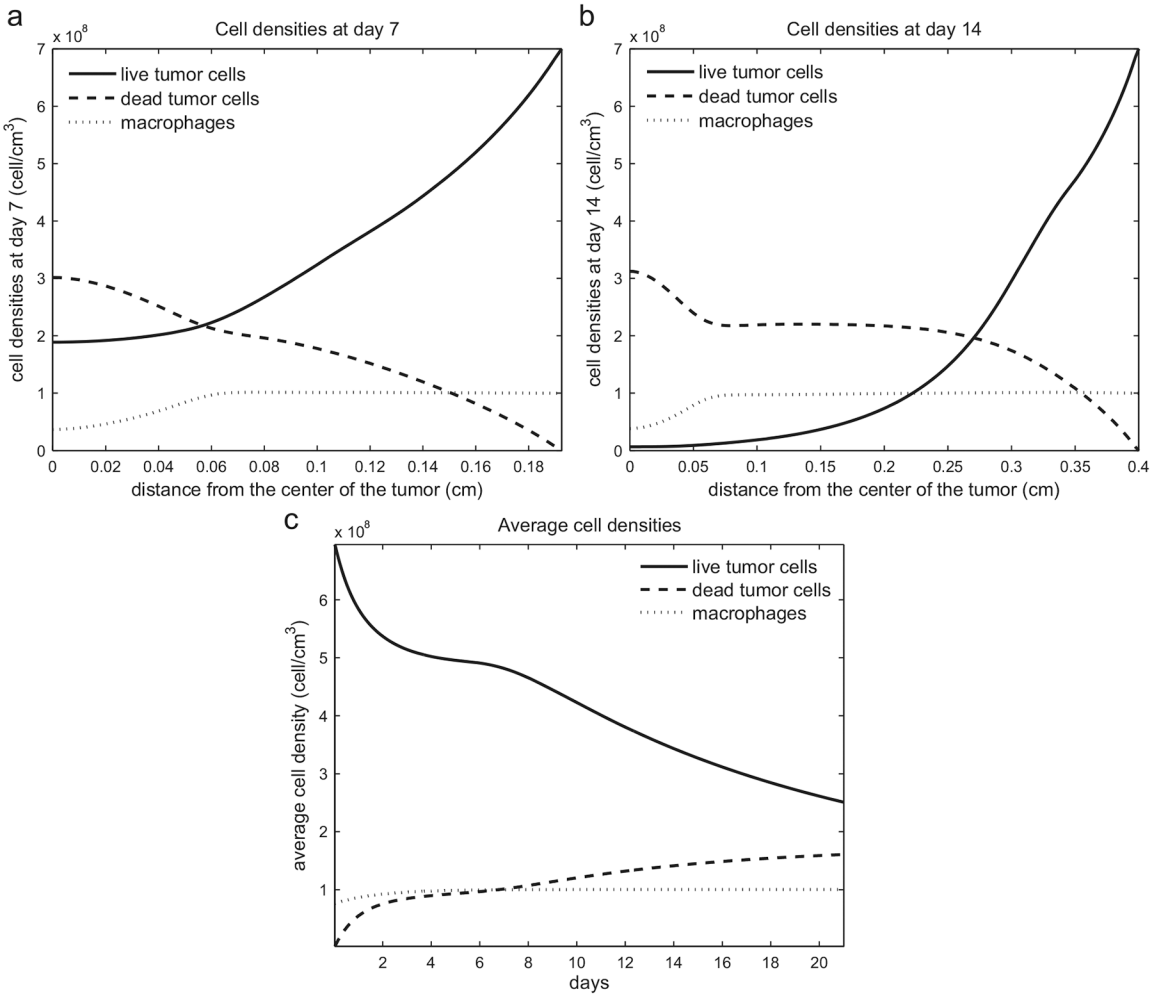

Fig. 2.

(a) Tumor cell (live and dead) and macrophage densities at day 7, when the tumor radius is 0.207 cm. (b) Tumor cell and macrophage densities at day 14, when the tumor radius is 0.41 cm. (c) Average cell densities over time.

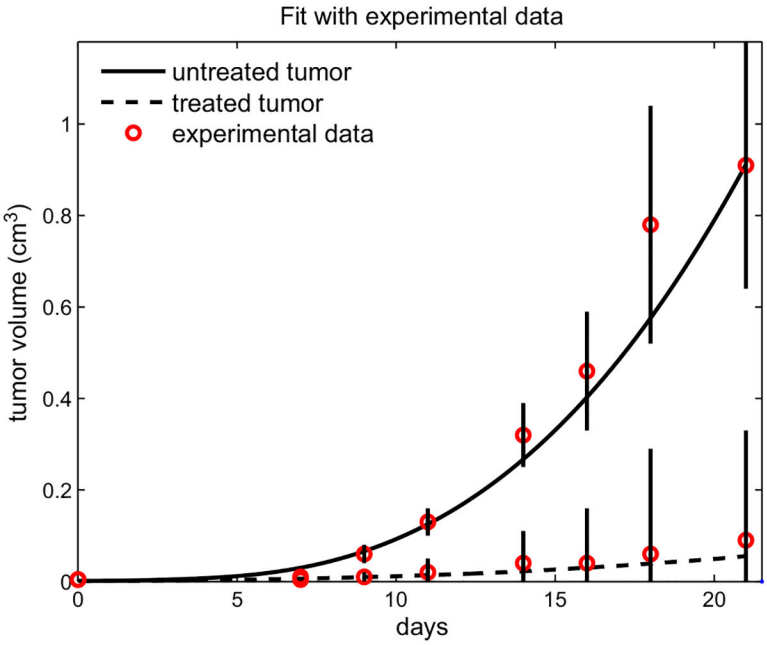

Fig. 3.

The volume of the treated and untreated tumor during 21 days. The circles and vertical lines correspond to experimental data and standard deviations from (Eubank et al., 2008).

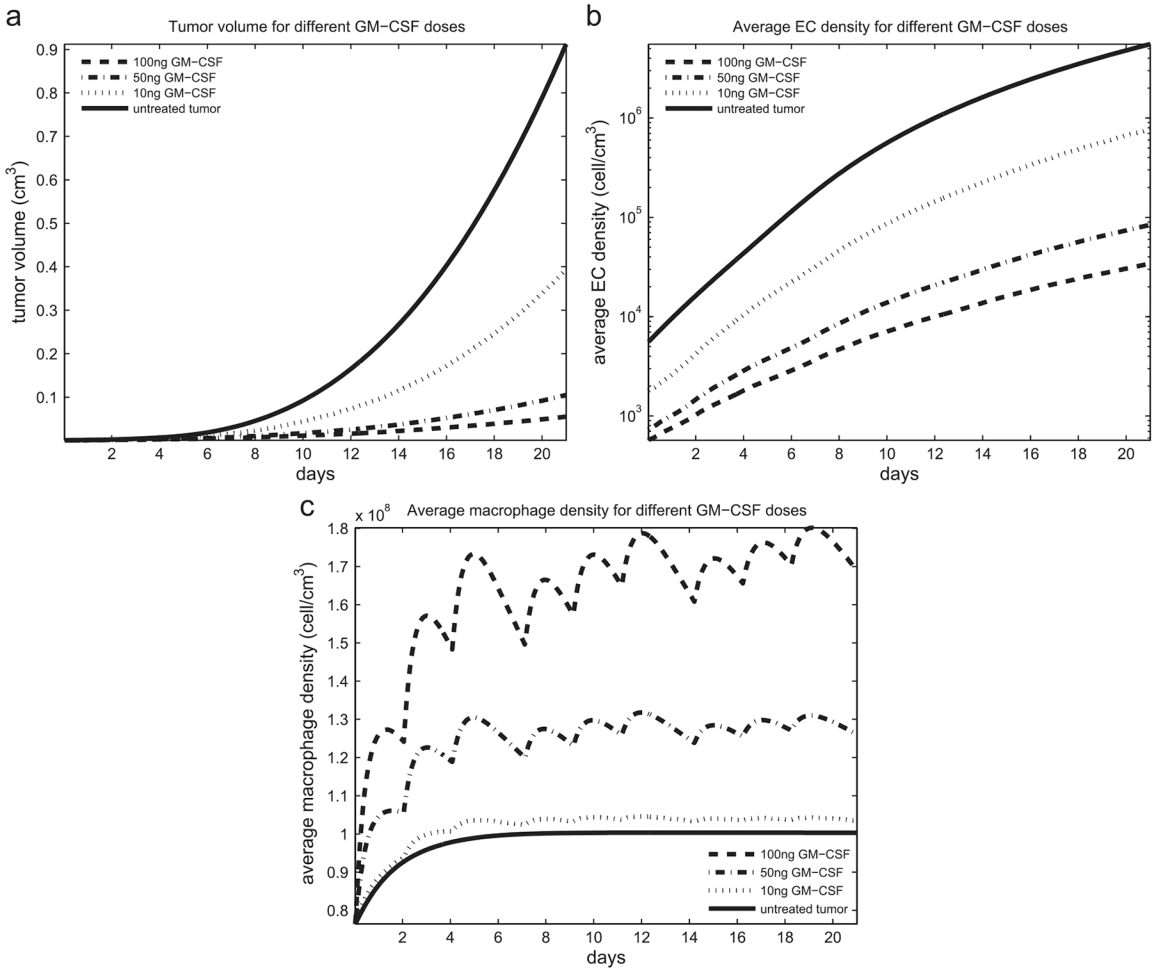

Fig. 4.

(a) Tumor volume; (b) average endothelial cell density; (c) average macrophage density for different doses of GM-CSF.

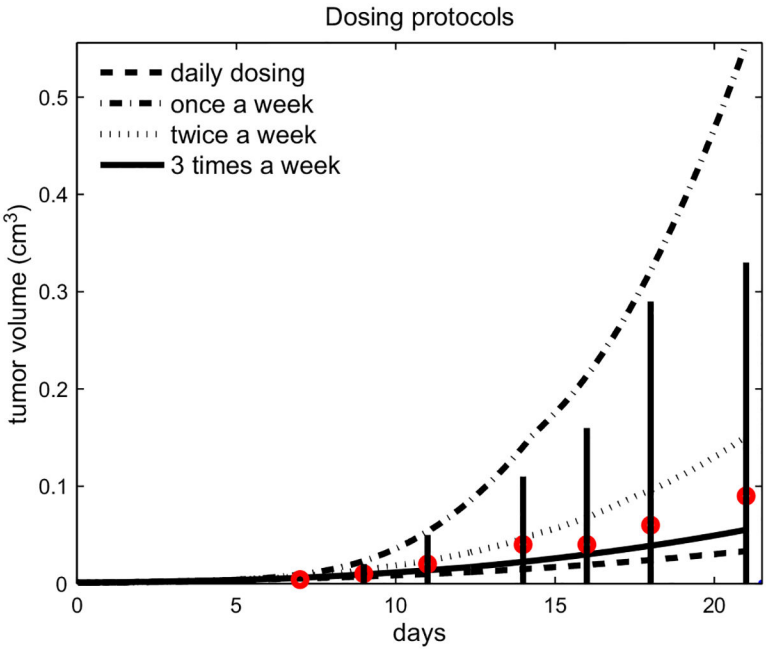

Fig. 5.

Comparing the tumor volume under different dosing protocols (daily, weekly, twice a week, three times a week) with the same total amount of GM-CSF in comparison with the experimental data from Eubank et al. (2008), where the dosing was three times a week.

Table 1

Model variables.

c	Live tumor cell density (cell cm^{-3})
b	Dead tumor cell density (cell cm^{-3})
w	Oxygen density (g cm^{-3})
e	Endothelial cell density (cell cm^{-3})
h	VEGF density (g cm^{-3})
s	M-CSF density (g cm^{-3})
m	Macrophage density (cell cm^{-3})
p	MCP-1 density (g cm^{-3})
g	GM-CSF density (g cm^{-3})

J Theor Biol. Author manuscript; available in PMC 2019 November 18.

Table 2

Parameter values.

Parameter	Dimensional value	Dimensionless value	Reference
D_c	10^{-10} cm^2 s^{-1}	10^{-4}	Owen et al. (2004), and estimated
D_b	10^{-10} cm^2 s^{-1}	10^{-4}	Estimated
D_m	5×10^{-11} cm^2 s^{-1}	5×10^{-5}	Owen et al. (2004)
D_h	5×10^{-7} cm^2 s^{-1}	0.5	Schugart et al. (2008)
D_e	10^{-11} cm^2 s^{-1}	10^{-5}	Owen et al. (2004), Plank et al. (2004), and estimated
D_w	5×10^{-7} cm^2 s^{-1}	0.5	Schugart et al. (2008), Owen et al. (2004)
D_s	10^{-6} cm^2 s^{-1}	1	Estimated
D_p	10^{-6} cm^2 s^{-1}	1	Owen et al. (2004), Owen and Sherratt (1997), and estimated
D_g	5×10^{-8} cm^2 s^{-1}	0.05	Caldwell et al. (1991), and estimated
λ_1	10^{-5} s^{-1}	2.53	Owen et al. (2004) and Qian et al. (2009)
λ_2	7×10^{-16} g s^{-1} cell^{-1}	0.93	Estimated
λ_3	7×10^{-13} cm^3 s^{-1} cell^{-1}	35	Girgis-Gabardo and Hassell (2008)
λ_4	4×10^{-13} cm^3 s^{-1} cell^{-1}	70	Butterworth and Cater (1967), Chen et al. (2009), and estimated
λ_5	7×10^{-6} s^{-1}	1.74	Chaplain et al. (1995), and estimated
λ_6	2.12×10^{-22} g s^{-1} cell^{-1}	3.72	Braunstein et al. (2007), Owen et al. (2004), Owen and Sherratt (1997), Pyaskovskaya et al. (2008), and estimated
λ_7	1.48×10^{-21} g s^{-1} cell^{-1}	7.43	Melillo et al. (1999), Vicioso et al. (2006), and estimated
λ_8	4×10^5 cm^3 g^{-1} s^{-1} cell^{-1}	8×10^5	Estimated
λ_9	3.18×10^{-22} g s^{-1} cell^{-1}	5.57	Oren et al. (2001), Utting et al. (2010), and estimated
λ_{10}	1.48×10^{-21} g s^{-1} cell^{-1}	7.43	Bosco et al. (2004), and estimated
k_h	1 cm^5 g^{-1} s^{-1}	0.01	Schugart et al. (2008)
k_p	6 cm^5 g^{-1} s^{-1}	0.06	Owen et al. (2004)
k_g	0.909 cm^5 g^{-1} s^{-1}	0.0091	Estimated
w_h	1.07×10^{-4} g cm^{-3}	0.23	Vaupel et al. (2003), and estimated
w_n	3.35×10^{-5} g cm^{-3}	0.072	Vaupel et al. (2003), and estimated
w_0	4.65×10^{-4} g cm^{-3}	1	Vaupel et al. (2003)
a_1, h_0	10^{-8} g cm^{-3}	1	Schugart et al. (2008)

Parameter	Dimensional value	Dimensionless value	Reference
c_0	7×10^8 cell cm^{-3}	1	Vincensini et al. (2007) and Eubank et al. (2008)
m_0	2×10^8 cell cm^{-3}	1	Eubank et al. (2008)
c^*	9.45×10^8 cell cm^{-3}	1.35	Estimated
h_1	3.65×10^{-10} g cm^{-3}	0.036	Chaplain (1995), and estimated
m_1, m_c	10^8 cell cm^{-3}	0.5	Eubank et al. (2008)
e_1	5×10^6 cell cm^{-3}	2	Estimated
μ_c	5×10^{-6} s^{-1}	1.26	Breward et al. (2001)
μ_b	5×10^{-14} cm^3 s^{-1} cell^{-1}	2.53	Breward et al. (2001), and estimated
μ_h	1.26×10^{-4} s^{-1}	31.6	Plank et al. (2004)
μ_s	4.8×10^{-5} s^{-1}	12	Tang (2000)
μ_g	1.6×10^{-5} s^{-1}	4	Williams et al. (1999)
μ_p	2×10^{-5} s^{-1}	5	Owen and Sherratt (1997)
$\alpha_{2,3}$	10^{-10} g cm^{-3}	0.01	Estimated
α_4	2.5×10^5 cell cm^{-3}	0.1	Estimated
α_5	2.5×10^4 cell cm^{-3}	0.01	Estimated
γ_1	2 cm^{-1}	1	Estimated
γ_2	0.2 cm^{-1}	0.1	Estimated
ϵ	0.05 cm	0.1	Estimated
e_0	2.5×10^6 cell cm^{-3}	1	Scaling parameter, Less et al. (1991), Levine and Nilsen-Hamilton (2006), Hashizume (2000)
τ	2.5×10^5 s	1	Scaling parameter, estimated
L	0.5 cm	1	Scaling parameter, estimated
s_0, p_0, g_0	10^{-8} g cm^{-3}	1	Scaling parameter, estimated

J Theor Biol. Author manuscript; available in PMC 2019 November 18.

Table 3

Ten parameters chosen for sensitivity analysis and their ranges.

Parameter	Minimum	Baseline	Maximum	Units
θ_c	0.65	0.7	0.75	
D_b	5×10^{-11}	10^{-10}	5×10^{-10}	$cm^2\ s^{-1}$
w_1	4.02×10^{-5}	5.36×10^{-5}	8.04×10^{-5}	$g\ cm^{-3}$
λ_9	1.6×10^{-22}	3.2×10^{-22}	4.8×10^{-22}	$g\ s^{-1}\ cell^{-1}$
γ_2	0	0.2	2	cm^{-1}
λ_4	2.86×10^{-13}	4×10^{-13}	5.14×10^{-13}	$cm^3\ s^{-1}\ cell^{-1}$
θ_m	0.15	0.2	0.25	
λ_1	8.02×10^{-6}	10^{-5}	1.07×10^{-5}	s^{-1}
γ_1	1	2	4	cm^{-1}
c^*	9.1×10^8	9.45×10^8	9.8×10^8	$cell\ cm^{-3}$